α–MHC–βARK1–minigene–SV-40. The transgenes were linearized and purified before microinjection.
12. C. A. Milano *et al.*, *Proc. Natl. Acad. Sci. U.S.A.* **91**, 10109 (1994).
13. Institutional review board approval for all mouse experiments was obtained at Duke University, the University of Houston, and the University of California at San Diego.
14. Sarcolemmal membranes (*20*) were prepared from control mouse hearts, and competition binding isotherms were determined for the β_2-selective ligand ICI 118,551 [erythro-dl-1-(7-methylindan-4-yloxy)-3-isopropylaminobutan-2-ol] against the nonselective ligand ^{125}I-cyanopindolol (^{125}I-CYP). Two binding populations were thus identified: 25% high affinity [K_i (inhibition constant) = 0.9 nM; β_2 subtype] and 75% low affinity (K_i = 390 nM; β_1 subtype). Subsequent isoproterenol-binding isotherms (*21*) contained 75 nM ICI 118,551 in order to selectively study β_1AR binding.
15. S. A. Green, B. D. Holt, S. B. Liggett, *Mol. Pharmacol.* **41**, 889 (1992).
16. A. De Lean, J. M. Stadel, R. J. Lefkowitz, *J. Biol. Chem.* **255**, 7106 (1980); R. A. Cerione *et al.*, *Biochemistry* **23**, 4519 (1984).
17. R. S. Kent, A. De Lean, R. J. Lefkowitz, *Mol. Pharmacol.* **17**, 14 (1980).
18. H. A. Rockman *et al.*, *Proc. Natl. Acad. Sci. U.S.A.* **91**, 2694 (1994).
19. H. A. Rockman *et al.*, unpublished data.
20. Myocardial sarcolemmal membranes were prepared by homogenization of whole hearts in ice-cold buffer A [50 mM Hepes (pH 7.3), 150 mM KCl, and 5 mM EDTA]. Nuclei and tissue were separated by centrifugation at 800*g* for 10 min and the crude supernatant was then centrifuged at 20,000*g* for 10 min. Sedimented proteins were resuspended at a concentration of 2 to 3 mg protein per milliliter in buffer B [50 mM Hepes (pH 7.3), and 5 mM $MgCl_2$].
21. Competition binding isotherms in sarcolemmal membranes (*20*) were done with 80 pM ^{125}I-CYP and varying amounts of isoproterenol in 250 μl of binding buffer [50 mM Hepes (pH 7.3), 5 mM $MgCl_2$, 0.1 mM ascorbic acid, and 75 nM ICI 118,551] with or without 100 μM GTP. Assays were done at 37°C for 1 hour and then filtered over glass fiber filters, which were washed twice and counted in a gamma counter. Data were analyzed by nonlinear least-square curve fitting [P. J. Munson and D. Rodbard, *Anal. Biochem.* **107**, 220 (1980)]. The data in Fig. 3A could not be fitted to the same parameters and represent the best simultaneous fit of the data with shared high- and low-affinity values.
22. We prepared myocardial extracts essentially as described (*6*) by homogenization of whole hearts in ice-cold lysis buffer (2 ml) [25 mM tris-HCl (pH 7.5), 5 mM EDTA, 5 mM EGTA, leupeptin (10 μg/ml), aprotinin (20 μg/ml), and 1 mM phenylmethylsulfonyl fluoride]. The crude homogenate was centrifuged for 30 min at 20,000*g*. Sedimented material was discarded and protein concentrations of the supernatants were determined [M. M. Bradford, *Anal. Biochem.* **72**, 248 (1976)]. TGβK heart samples were further purified by addition of NaCl (to a final concentration of 50 mM) and 0.75 ml of a slurry of 50% (v/v) diethylaminoethyl Sephacel (pH 7.0). This mixture was incubated on ice for 30 min and poured over a small disposable column. Final supernatants were eluted with 1 ml of cold lysis buffer and concentrated with a Centricon (Amicon) microconcentrator. βARK1-minigene expression was assessed directly from concentrated supernatants.
23. Total RNA was extracted with RNAzol (Biotecx Laboratories, Houston, TX) [P. Chomczynski and N. Sacchi, *Anal. Biochem.* **162**, 156 (1987)].
24. GRK activity of heart extracts was determined in concentrated supernatants from TGβK and control mice (*22*). Extracts (50 μg protein) were incubated with rhodopsin-enriched rod outer segments (*8*) in lysis buffer (75 μl) (*22*) with 10 mM $MgCl_2$ and 0.1 mM adenosine triphosphate (ATP) (containing [γ-^{32}P]ATP). After incubation in white light for 15 min at room temperature, reactions were quenched with ice-cold lysis buffer (300 μl) and centrifuged for 15 min at 13,000*g*. The sedimented proteins were resuspended in 20 μl of lysis buffer and electrophoresed on 12% SDS-polyacrylamide gels. The gels were dried and phosphorylated rhodopsin was quantitated with a PhosphorImager (Molecular Dynamics).
25. Y. Salomon, C. Londos, M. Rodbell, *Anal. Biochem.* **58**, 541 (1974).
26. Mice were anesthetized with a mixture of ketamine and xylazine (*7*). After endotracheal intubation, mice were connected to a volume-cycled ventilator. Either carotid artery was cannulated with a flame-stretched PE 50 catheter connected to a modified P50 statham transducer. The chest was then opened and a 2F high-fidelity micromanometer catheter was inserted into the left atrium, advanced through the mitral valve, and secured in the LV. Hemodynamic measurements were recorded at baseline and 45 to 60 s after injection of incremental doses of isoproterenol. Continuous pressures were recorded on an eight-channel chart recorder and in digitized form on computer disk for beat averaging. Ten sequential beats were averaged for each measurement.
27. We thank J. Robbins for the murine α-MHC promoter; C. Bock, W. C. Stone, and N. Rahman for technical assistance; M. Tiberi for assistance in computer analysis; N. Freedman and P. Dolber for helpful discussions during the course of this work; and D. Addison and M. Holben for secretarial assistance. Supported in part by NIH grants HL-16037 (R.J.L.) and 5F32-CA09350 (C.A.M.) and by the American Heart Association, California affiliate grant 94G-286 (H.A.R.) and Texas affiliate grant 94G-458 (R.A.B.).

3 January 1995; accepted 7 March 1995

Sensorimotor Encoding by Synchronous Neural Ensemble Activity at Multiple Levels of the Somatosensory System

Miguel A. L. Nicolelis,*† Luiz A. Baccala, Rick C. S. Lin, John K. Chapin

Neural ensemble processing of sensorimotor information during behavior was investigated by simultaneously recording up to 48 single neurons at multiple relays of the rat trigeminal somatosensory system. Cortical, thalamic, and brainstem neurons exhibited widespread 7- to 12-hertz synchronous oscillations, which began during attentive immobility and reliably predicted the imminent onset of rhythmic whisker twitching. Each oscillatory cycle began as a traveling wave of neural activity in the cortex that then spread to the thalamus. Just before the onset of rhythmic whisker twitching, the oscillations spread to the spinal trigeminal brainstem complex. Thereafter, the oscillations at all levels were synchronous with whisker protraction. Neural structures manifesting these rhythms also exhibited distributed spatiotemporal patterns of neuronal ensemble activity in response to tactile stimulation. Thus, multilevel synchronous activity in this system may encode not only sensory information but also the onset and temporal domain of tactile exploratory movements.

The processing of somatosensory information in the mammalian brain involves the transmission of neural activity from the skin to the neocortex by way of parallel pathways that ascend through a hierarchical sequence of neural structures (*1*). Like those in other sensory systems, these ascending pathways are far outnumbered by corticofugal descending projections (*2*), which can act at multiple subcortical levels to modify the processing of sensory information (*3*). These connections define a recurrent network that is theoretically capable of generating complex emergent dynamic patterns of neural activity, manifested by synchronous oscillations or even chaotic behavior (*4*), that could be computationally useful (*5*). The existence of this network raises the question of whether large-scale coordinated activity of neural ensembles involving multiple levels of a sensory system (that is, brainstem, thalamus, and cortex) can play a fundamental role in the coding of sensory information. To address this issue, we simultaneously recorded up to 48 single neurons, distributed across up to five distinct processing relays of the trigeminal somatosensory system, in freely behaving rats (*6*). The rat trigeminal system is a multilevel, recurrently interconnected neuronal network, specialized for processing complex patterns of tactile stimuli generated by the repetitive contacts of facial whiskers with surrounding objects. Rats rely on rhythmic movements of their facial whiskers, much as humans rely on coordinated movements of their fingertips, to discriminate object shape and texture (*7*). Although the properties of single neurons belonging to this sensory system have been well studied under anesthetized con-

M. A. L. Nicolelis, R. C. S. Lin, J. K. Chapin, Department of Anatomy and Neurobiology, Medical College of Pennsylvania and Hahnemann University, Philadelphia, PA 19102, USA.
L. A. Baccala, Department of Electrical Engineering, University of Pennsylvania, Philadelphia, PA 19104, USA, and Department of Electronic Engineering, University of São Paulo, São Paulo, SP, Brazil.

*Present address: Department of Neurobiology, Box 3209, Duke University Medical Center, Durham, NC 27710, USA.
†To whom correspondence should be addressed.

ditions (8), little is known about information processing at the neural ensemble level during exploratory tactile behaviors.

The results described here are based on the long-term behavior of 424 single neurons chronically recorded in 11 animals. Sampled structures included the trigeminal ganglion (Vg, 17 cells), the principal (PrV, 52 cells) and spinal (SpV, 39 cells) trigeminal brainstem nuclei, the ventral posterior medial (VPM, 186 cells) and posterior medial (POm, 19 cells) nuclei of the thalamus, the primary somatosensory (SI, 95 cells) cortex, and the primary motor (MI, 32 cells) cortex. Pairwise cross correlation analysis was initially used to characterize the coordinated activity of simultaneously recorded neurons across the trigeminal system. Cross correlograms averaged around the spiking of a single representative VPM neuron (Fig. 1A) in each animal demonstrated the existence of synchronous oscillatory discharges (7 to 12 Hz) in 98% of the ipsilateral VPM neurons, 92% of the ipsilateral SI cortical neurons, and 49% of the contralateral SpV neurons recorded in this study. During episodes of synchronous firing, thalamic neurons tended to phase-lag (follow) cortical neurons (Fig. 1A) by time periods ranging from 0 to 20 ms (mean ± SD, 9.19 ± 4.67 ms; $n = 84$ SI-VPM pairs in six animals). The regular progression of these lags across evenly spaced electrode arrays implanted in the SI cortex (for an example see the bottom third of Fig. 1A) was compatible with a traveling wave of neuronal activity crossing this cortical region. Similar synchronous oscillations were also observed among neurons in the whisker representation of the rat MI cortex, and, like the SI cortical neurons, these neurons phase-led neurons in the VPM thalamus. The simultaneously recorded neurons in the brainstem SpV nucleus were also synchronized with this oscillation, and these neurons phase-led neurons in the VPM thalamus by as much as 40 ms (Fig. 1A). By contrast, neurons within the VPM and POm thalamus exhibited remarkably synchronous firing with minimal phase lags (<3 ms). This high degree of synchrony was observed bilaterally in the thalamus, implying that all of these thalamic structures were simultaneously entrained into the oscillations.

The possibility that these oscillations were caused by rhythmic sensory feedback resulting from active whisker movements (WMs) was ruled out by three observations. First, as detailed below, they began well before the onset of WMs. Second, the same pattern of oscillations was clearly present in adult animals subjected to complete unilateral whisker removal or facial nerve section in early development (9). Third, the oscillations were not observed in either the first-order (Vg) or the primary second-order (PrV) sensory relays in this pathway.

To further examine the neurophysiological properties of the simultaneously recorded multilevel neural ensembles, we developed analytical techniques for representation of neuronal population functions. We used principal components analysis (PCA) to construct continuous representations of the activity of neuronal populations by weighted summation of the time-integrated activity of all neurons (*10*). We observed that reconstructions of the first principal component (PC1), derived from combined cortical, thalamic, and brainstem neural ensemble activity,

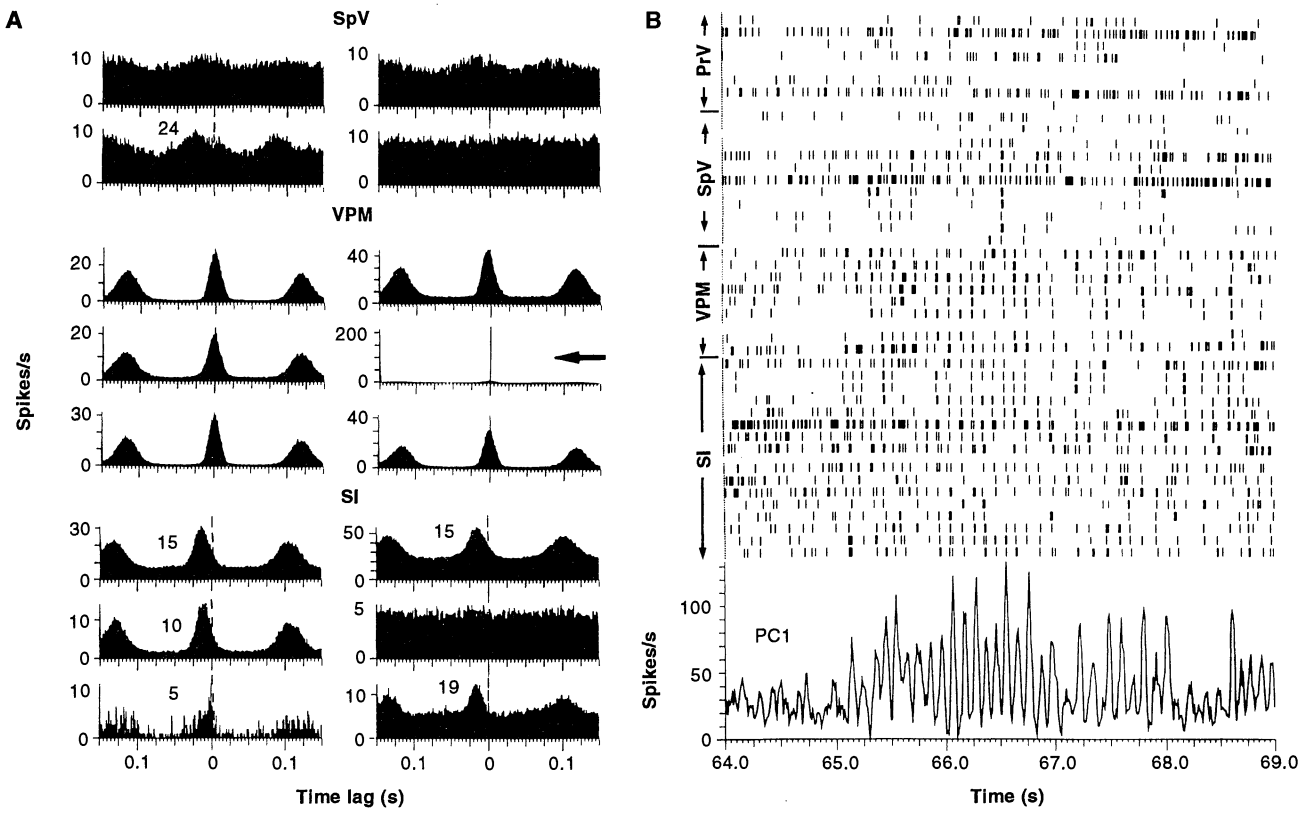

Fig. 1. Spontaneous 7- to 12-Hz oscillations at multiple relays of the trigeminal somatosensory system. (**A**) Cross correlograms (CCs), calculated for 16 out of a total 48 simultaneously recorded neurons, reveal synchronous 7- to 12-Hz oscillations at three levels of the trigeminal pathway (SpV, 4 neurons; VPM, 6 neurons; and SI, 6 neurons). All CCs centered around the spiking of one reference VPM neuron (autocorrelation shown at arrow). Numbers on top of CCs indicate the time interval (in milliseconds) by which each SpV or SI neuron phase-leads the reference VPM neuron. All horizontal axes indicate pre- and post-VPM spike times (in seconds). VPM spiking occurred at 0.0 s, as indicated by the vertical dashed lines. Vertical axes of CCs indicate equivalent firing rates per bin (bins: 1-ms duration). (**B**) Continuous strip chart showing 43 single-unit rasters and reconstructed PC1 (bottom) over the same 5.0-s time period in an awake rat. The rasters show spiking activity of simultaneously recorded neurons in four system relays; PrV, SpV, VPM, and SI. Not shown are the five neurons recorded in Vg, which were inactive over this period. The vertical axis depicts the weighted neuronal population firing rate.

more reliably identified the existence and time course of oscillatory episodes than did the raster displays of single neuronal spiking (Fig. 1B). This difference was due to the marked variability in spiking patterns (timing and number of spikes) of single neurons over different oscillatory cycles. Indeed, only a fraction of the population fired during a particular cycle. Thus, oscillations revealed in PC1 were not completely defined by any one neuron but instead drew small amounts of variance from each of a large population of neurons. Because PC1 normally explains the most global sources of covariance between variables, it is significant that it tended to be dominated by these widespread synchronous oscillations (*11*).

Spectrum analysis of the time series representing PC1 for the multilevel data demonstrated that the most important power contribution of the oscillations was in the frequency band from 7 to 12 Hz, with a secondary peak at 19 to 21 Hz. The oscillations appeared in episodes ranging from 0.8 to 38.2 s (mean ± SE, 3.96 ± 0.3 s; n = 196 episodes) and were closely associated with preparation for movement (Fig. 2). Although they always began during complete immobility (Fig. 2A), in 79.1% (155 of 196, from five animals) of the recorded episodes, these oscillations predicted with a high degree of statistical confidence ($P < 10^{-6}$) the imminent onset of low-amplitude whisker-twitching (WT) movements (*12*). Even though WT began on average 581 ± 45.2 ms after the oscillation onset, the distribution of these latencies was markedly skewed, such that 62.5% of all WT episodes began during the first 500 ms. The frequency range of WT (7) closely matched the frequency of neural oscillations in the trigeminal system (7 to 12 Hz). In fact, after the onset of WT, these oscillations assumed a phase-locked relation with this movement: Oscillatory peaks in the SpV were synchronous with the early phase of whisker protraction, whereas peaks in the SI and VPM were synchronous with the middle and late phases of whisker protraction, respectively (Fig. 2B). Subsequent onset of high-amplitude rhythmic exploratory WMs, which were often combined with head movements or locomotion, always induced a cessation of these oscillations. In the absence of WT, head movements (HMs) alone were never preceded by oscillations (see HMs starting at 13.7 s in Fig. 2A). Independent reconstruction of principal components (PCs) at different levels of the trigeminal pathway revealed that in 79.8% (138 of 173, n = five animals) of the oscillatory sequences, rhythmic activity clearly began in the SI cortex (Fig. 3A, point a) and progressed to the VPM thalamus (Fig. 3A, point b). Neurons in the SpV tended to be recruited last, exhibiting clear rhythmic activity 1.53 ± 0.07 oscillatory cycles (~100 ms per cycle) before the onset of WT (Fig. 3A, dashed line), as averaged across 114 episodes in which SpV neurons were recorded (Fig. 3A, point c). Although the SpV neurons were the last to be recruited into rhythmic activity, after the onset of WT they phase-led both the SI and VPM neurons (Figs. 2B and 3B). This observation argues against a simple pacemaker mechanism for these oscillations.

The classification of this oscillatory phenomenon remains elusive (*13*). Its association with attentive behaviors resembles that of "mu" rhythms recorded in humans (*14*) and the "sensorimotor" rhythms described in cats and primates (*15*). Our data suggest that similar oscillatory activity is present at multiple processing levels of the rat somatosensory system and that it can be definitively related to a specific type of rhythmic movement (WT). Differences in the frequency of this rhythm across species might therefore be related to different time domains of movements for which it is preparatory. Our hypothesis is that the 7- to 12-Hz frequency component of the oscillations defines an "internally generated representation" of the sensorimotor temporal domain of exploratory movements, especially WT, which is disseminated across

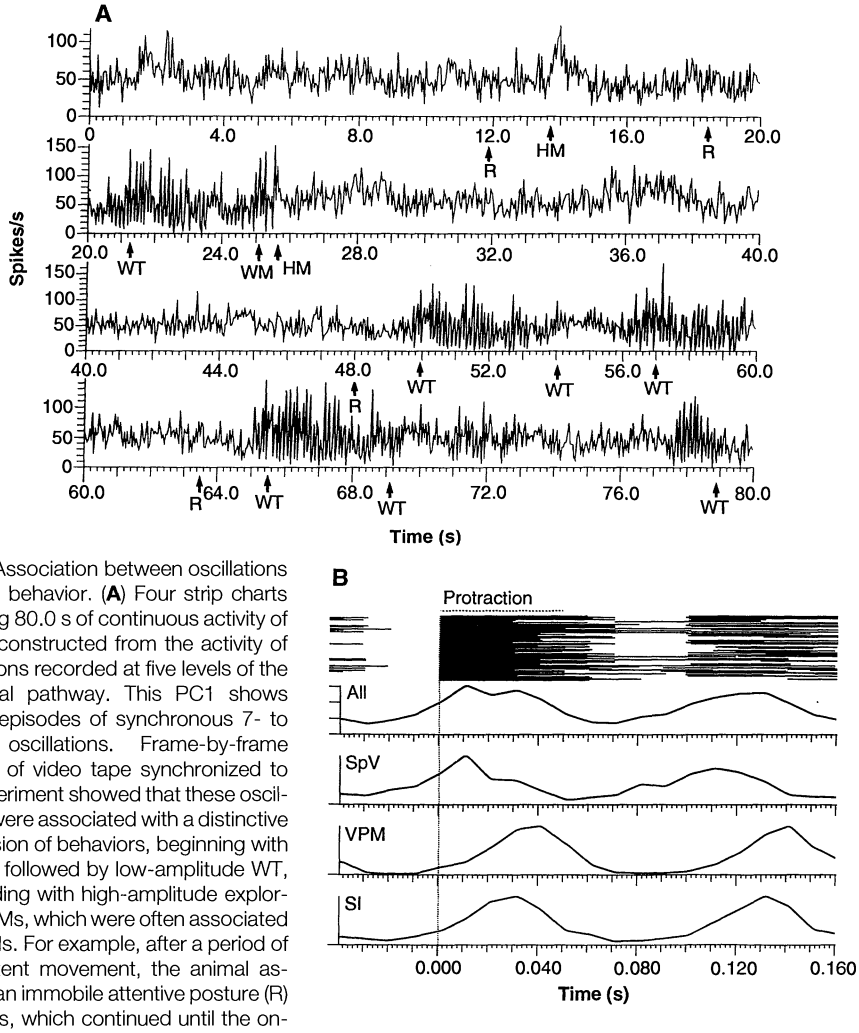

Fig. 2. Association between oscillations and WT behavior. (**A**) Four strip charts depicting 80.0 s of continuous activity of PC1, reconstructed from the activity of 48 neurons recorded at five levels of the trigeminal pathway. This PC1 shows several episodes of synchronous 7- to 12-Hz oscillations. Frame-by-frame analysis of video tape synchronized to this experiment showed that these oscillations were associated with a distinctive succession of behaviors, beginning with rest (R), followed by low-amplitude WT, and ending with high-amplitude exploratory WMs, which were often associated with HMs. For example, after a period of intermittent movement, the animal assumed an immobile attentive posture (R) at 18.5 s, which continued until the onset of oscillations (7 to 12 Hz) at 20.5 s. About 500 ms later, a sequence of low-amplitude WT (21.2 to 25.1 s) began. This WT was then followed by WM and HM, which terminated the oscillations. Vertical arrows mark the onset of various behaviors. (**B**) Phase synchronization between whisker protraction and 7- to 12-Hz oscillations at multiple levels of the trigeminal system. A raster plot (top) and PC1s (for different levels) are shown centered around the onsets of 64 episodes of whisker protraction during WT. Each black horizontal line in the raster defines the time period between protraction onset (vertical dotted line at 0.0 s) and subsequent retraction onset. The horizontal dotted line above the raster plot depicts the average duration (49 ms) of whisker protraction during continuous WT. The PC1s calculated for all levels together (topmost PC1 plot) or for each individual level (SpV, VPM, and SI) are averaged around the onset of whisker protraction. All PC1s are tightly phase-locked to whisker protraction, and the SpV, SI, and VPM activity peaks occur during the early, middle, and late phases of protraction, respectively. The vertical axis depicts the weighted neuronal population activity.

much of the somatosensory pathway before the onset of the movement.

We propose that these synchronous oscillations provide a phasic sensory facilitation function timed to coincide with whisker protraction, which is known to be the period in which active sampling of tactile information occurs in rats (*7*). In this model, the observed 19- to 21-Hz frequency component might constitute a representation of the timing of alternating subphases of WM—for example, protraction and retraction (Fig. 2B). Further support for this model is provided by our observation that, depending on the oscillatory phase at which the incoming sensory volley arrives, these rhythms can modify the response to the stimulus (Fig. 3C).

The strong correlation of these sensorimotor rhythms with immobile attention leading to WT clearly distinguishes these rhythms from other brain rhythms such as spindling (*16*). To further clarify this distinction, we compared the sensorimotor rhythms with spindling activity in the same animals and found that there were several differences between these two rhythms. First, spindles occurred during drowsiness (as opposed to attentive resting) and during the initial stages of sleep, in the complete absence of WMs. Second, oscillatory sequences during spindling occurred in much shorter (0.4 to 1.2 s) and stereotyped episodes than did the sensorimotor rhythms described during awake immobility. Third, unlike the relatively constant amplitude of the sensorimotor oscillations, the spindles exhibited very characteristic waxing and waning wave patterns. Finally, spindle episodes recurred every 5 to 10 s, whereas the occurrence of sensorimotor rhythms was linked to behavior changes and was therefore more random. Thus, although spindles involved similar frequencies (7 to 14 Hz) and were observed in the same thalamocortical circuits, they clearly subserve a very different functional role from the sensorimotor rhythms described here.

To further define the dynamic nature of sensory processing among the multiple processing levels of the rat trigeminal system during awake immobility, we carried out repetitive stimulation of single whiskers in the same animals. Population poststimulus time histograms (PPSTHs) were used to represent the simultaneously recorded sensory responses of the same ensemble of neurons to repeated stimulation of a given whisker (Fig. 4). This analysis revealed that Vg and PrV neurons (1 to 13 in the vertical scale of Fig. 4) responded well to the stimulation of a single whisker (B4, Fig. 4B) but exhibited little or no response to stimulation of other sites (such as whisker B2, Fig. 4A, and fur rostral to B4, Fig. 4C). In contrast, most of the SpV (14 to 22), VPM (23 to 31), and SI (32 to 47) neurons displayed statistically significant ($P < 0.01$) responses to all three stimulation sites. In the ascending progression from Vg to SI, the latencies to the initial response increased from 2 to 8 ms. In addition, secondary long-latency responses were evident through much of this system, appearing first in a few PrV neurons and becoming more prominent and longer in latency at higher levels. For instance, thalamic cells exhibited secondary long-latency responses up to 35 ms, and, in the SI cortex, secondary long-latency responses ranged from 20 to 70 ms after the stimulus. As previously demonstrated for the VPM neurons (*17*), these results showed that sensory maps at most

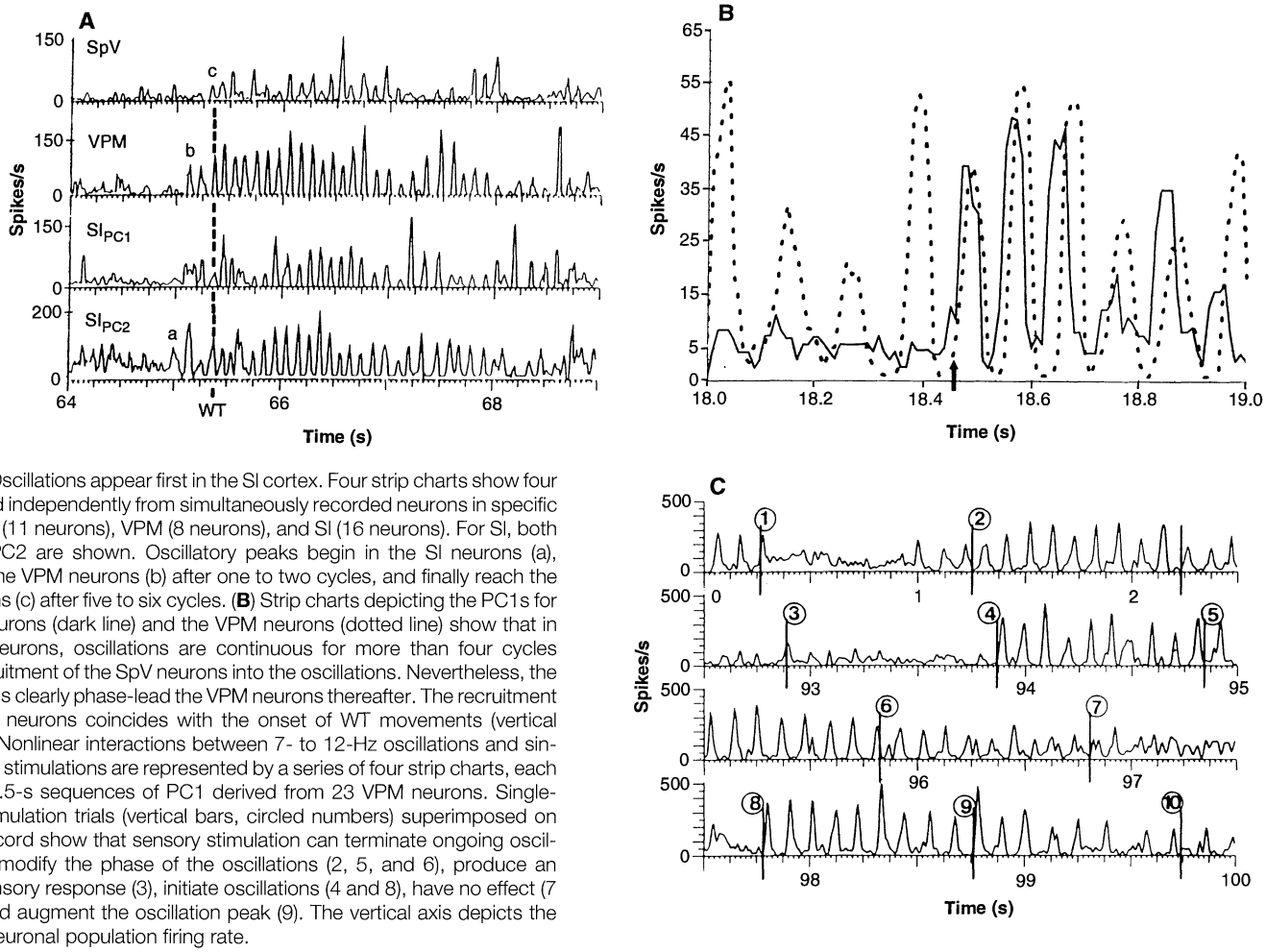

Fig. 3. (**A**) Oscillations appear first in the SI cortex. Four strip charts show four PCs derived independently from simultaneously recorded neurons in specific nuclei: SpV (11 neurons), VPM (8 neurons), and SI (16 neurons). For SI, both PC1 and PC2 are shown. Oscillatory peaks begin in the SI neurons (a), spread to the VPM neurons (b) after one to two cycles, and finally reach the SpV neurons (c) after five to six cycles. (**B**) Strip charts depicting the PC1s for the SpV neurons (dark line) and the VPM neurons (dotted line) show that in the VPM neurons, oscillations are continuous for more than four cycles before recruitment of the SpV neurons into the oscillations. Nevertheless, the SpV neurons clearly phase-lead the VPM neurons thereafter. The recruitment of the SpV neurons coincides with the onset of WT movements (vertical arrow). (**C**) Nonlinear interactions between 7- to 12-Hz oscillations and single-whisker stimulations are represented by a series of four strip charts, each depicting 2.5-s sequences of PC1 derived from 23 VPM neurons. Single-whisker stimulation trials (vertical bars, circled numbers) superimposed on the PC1 record show that sensory stimulation can terminate ongoing oscillations (1), modify the phase of the oscillations (2, 5, and 6), produce an isolated sensory response (3), initiate oscillations (4 and 8), have no effect (7 and 10), and augment the oscillation peak (9). The vertical axis depicts the weighted neuronal population firing rate.

levels of the trigeminal system (SpV, VPM, POm, and SI) were defined by complex spatiotemporal patterns of neural ensemble responses. Therefore, although the Vg and PrV structures contained relatively simple topographic sensory representations and did not exhibit premovement oscillations, structures that manifested synchronous oscillations (SpV, VPM, POm, and SI) exhibited distributed (*18*) and dynamic somatosensory maps.

The complex spatiotemporal structure of these maps may result from asynchronous interactions between feedforward and feedback projections at each level of this system. As a consequence, the coding of sensory information in most cortical and subcortical relays of the trigeminal pathways occurs at the ensemble rather than at the single-unit level and involves both spatial and temporal domains. According to this scenario, topographic maps defined in anesthetized animals represent only a first approximation of the system's functional organization. In the awake condition, however, spatiotemporal complexity substitutes for topography as the main strategy for the coding of sensory information.

These results indicate that the functional organization of the rat somatosensory system is fundamentally linked to the coordinated activity of large ensembles of neurons, distributed through multiple levels of the brain. Dynamic patterns of neural ensemble activity in this sensory system were found not only to code tactile stimulus attributes but also to anticipate the occurrence of stereotyped WT behaviors associated with active tactile exploration of the surrounding environment. Because these oscillations appear to mimic a motor output function, they are consistent with earlier demonstrations in rats, cats, and monkeys that the transmission of sensory information through different levels of the somatosensory system is strongly modulated as a function of the phase of active movement (*19*).

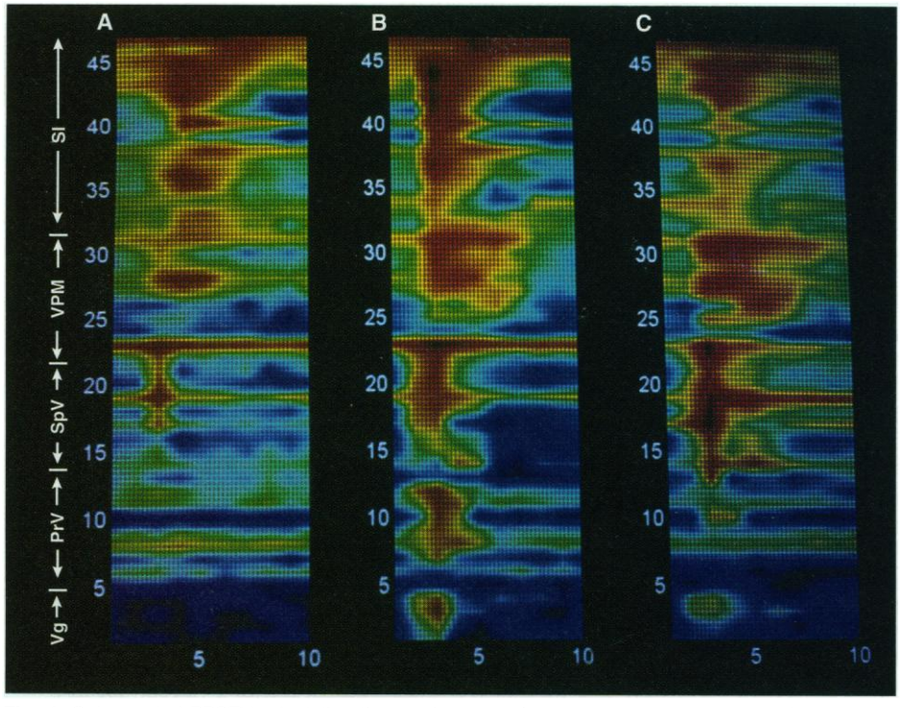

Fig. 4. Color-coded PPSTHs depicting the spatiotemporal sensory response patterns of 47 neurons simultaneously recorded across five levels of the trigeminal system in an awake rat. The absolute neuronal firing intensities are displayed through a seven-color contour plot [dark red, highest firing rate (up to 120 Hz); dark blue, lowest firing rate (as low as 0 Hz)]. Neurons that are included in this multilevel ensemble are organized in the vertical axis (Vg, 1 to 4; PrV, 5 to 13; SpV, 14 to 22; VPM, 23 to 31; and SI, 32 to 47). Poststimulus time is represented in 5-ms time bins numbered from 1 to 10 (0 to 50 ms). The graphs were produced by calculating the intensities of spike discharge of each neuron within the simultaneously recorded ensemble, rank-ordering the neurons into rows according to receptive field location, and then plotting the data into a color-coded contour plot image. Each PPSTH depicts the spatial extent and timing of the spread of sensory responses through the nuclei in which neuronal ensembles were simultaneously recorded. Sensory responses obtained for whisker B2 (**A**), whisker B4 (**B**), and fur rostral to B4 (**C**) are illustrated. All PPSTHs were based on 360 single-whisker stimulation trials. Each trial consisted of a 100-ms step pulse that produced a 3° whisker deflection (upward first). Raw data were smoothed with a spline algorithm (Matlab); the statistical significance of sensory responses was computed by means of a one-way Kolmogorov-Smirnov test.

REFERENCES AND NOTES

1. J. H. Kaas, in *The Human Nervous System*, G. Paxinos, Ed. (Academic Press, San Diego, CA, 1990), pp. 813–844.
2. S. M. Sherman and C. Koch, in *The Synaptic Organization of the Brain*, G. M. Shepherd, Ed. (Oxford Univ. Press, New York, 1990), pp. 246–278; I. T. Diamond and W. C. Hall, *Science* **164**, 251 (1969); J. Cmielowska, G. E. Carvell, D. J. Simons, *J. Comp. Neurol.* **285**, 325 (1989).
3. H.-C. Shin and J. K. Chapin, *Brain Res. Bull.* **22**, 245 (1989); *ibid.* **24**, 257 (1990); *Neurosci. Lett.* **108**, 116 (1990).
4. W. J. Freeman, *Mass Action in the Nervous System* (Academic Press, New York, 1975); _____ and B. Baird, *Behav. Neurosci.* **101**, 393 (1987); G. Laurent and H. Davidowitz, *Science* **265**, 1872 (1994).
5. H. Sompolinsky, D. Golomb, and D. Kleinfeld [*Phys. Rev. A* **43**, 6990 (1991)] have suggested that computations might be carried out by systems of coupled oscillators in which information is carried in changing patterns of synchronous coupling between these oscillators. Computation in Hopfield nets [J. Hopfield, *Proc. Natl. Acad. Sci. U.S.A.* **79**, 2554 (1982); _____ and D. W. Tank, *Science* **233**, 625 (1986)], which are recurrently connected artificial neural networks, involves a dynamic evolution of the system toward a steady state.
6. Eleven adult Long-Evans (hooded) rats (250 to 300 g) were used in this study. Surgical and recording procedures complied with NIH-recommended procedures for animal use and care. These procedures and methods for single-whisker stimulation and data analysis are fully described elsewhere [M. A. L. Nicolelis and J. K. Chapin, *J. Neurosci.* **14**, 3511 (1994)]. Briefly, bundles and arrays of 50-μm microwires (NBLABS, Dennison, TX) were implanted under pentobarbital anesthesia (50 mg per kilogram of body weight, intraperitoneal). Sets of 8 to 16 microwires were stereotaxically placed in up to five neuronal structures per animal. Teflon-coated stainless steel wires (0.007 inch) were also implanted in multiple facial muscles to obtain electromyograms (EMGs). Concomitant videotaping of the animal's activity was also used to define the timing of different behaviors and to correlate these events with patterns of ensemble activity. Recordings were obtained during awake immobility, active whisker exploration of the environment, locomotion, and sleep. We obtained synchronous recordings of neuronal, EMG, and video signals with the use of a multichannel neuronal processor (MNAP; Spectrum Scientific, Dallas, TX). A single computer clock (accuracy, 0.2 ms) was used to synchronize the acquisition of neuronal and video data. Each video field was stamped with the elapsed time in hundredths of a second. A Lafayette (Lafayette, IN) Super VHS video analysis system was used for post hoc field-by-field analysis of video recordings. The 60 field per second video sampling rate provides a 16.7-ms temporal resolution, and the synchronization with experimental data capture has a 10-ms resolution. In the ensemble data analysis we used the following computer programs: Analyze (J. K. Chapin); Stranger (Biographics, Winston-Salem, NC); CSS:Statistica (Statsoft, Tulsa, OK); and Matlab (Mathworks, Natick, MA).
7. G. E. Carvell and D. J. Simons, *J. Neurosci.* **10**, 2638 (1990).
8. J. K. Chapin and C. S. Lin, *J. Comp. Neurol.* **229**, 199 (1984); J. K. Chapin, *Exp. Brain Res.* **62**, 549 (1986); M. Armstrong-James and C. A. Callahan, *J. Comp. Neurol.* **303**, 211 (1991).
9. R. C. S. Lin, M. A. L. Nicolelis, M. E. Diamond, J. K. Chapin, *Soc. Neurosci. Abstr.* **19**, 106 (1993); M. A. L. Nicolelis, R. C. S. Lin, J. K. Chapin, *ibid.* **20**, 125 (1994).
10. PCA simplifies the analysis of the activity of large numbers of neurons by linearly combining their covariant activity over a large number of experimental time bins into a much smaller number of PCs that explain most of the covariance. The matrix of coefficients for axis rotation that defines each PC is then used to weight-sum the simultaneous time-integrated activities of all neurons into a single continuous "population function," which provides optimal

identification of moment-to-moment changes in the activity of the underlying "factor" defined by the PC. For example, we constructed the record in Fig. 1B by (i) dividing the 1813-s experiment into 181,300 10-ms time samples; (ii) measuring the spiking of each of the 48 simultaneously recorded neurons within each time sample; (iii) standardizing each data sample by subtracting the mean and dividing by the standard deviation; (iv) using these samples to construct a 48 by 48 covariance matrix; (v) performing PCA on this matrix; and (vi) using the PC1 eigenvector to weight-sum all the standardized data samples into a continuous population function, consisting of a time series containing a single data point for each 10-ms time bin in the experiment.

11. In contrast to the information derived from PC1, higher-order components (with successively lower eigenvalues) identified local sources of covariance, including phase differences between oscillations at different levels of the pathway and specific sensory information.
12. Chi-square analysis rejected the null hypothesis that there is no temporal relation between WT and the oscillations. This analysis involved comparing the experimentally derived distribution of WT onset times (quantized in 100-ms bins after the onset of oscillation) with the theoretical distribution of onset times that would be predicted by the null hypothesis (that is, a homogeneous distribution whose sum of counts equals the experimental sum). Because the experimental distribution was markedly skewed toward very short time delays after the onset of oscillation, a very high χ^2 was obtained (658; df = 32 bins), allowing rejection of the null hypothesis ($P < 10^{-6}$).
13. K. Semba, H. Szechtman, B. R. Komisaruk, *Brain Res.* **195**, 281 (1980); K. Semba and B. R. Komisaruk, *Neuroscience* **12**, 761 (1984); G. Buzsaki, *ibid.* **41**, 351 (1991).
14. H. Gastaut, *Rev. Neurol. (Paris)* **87**, 176 (1952); R. Kristeva-Feige *et al.*, *Neuroreport* **4**, 1291 (1993); R. Salmelin and R. Hari, *Neuroscience* **60**, 537 (1994).
15. A. Rougeul, J. J. Bouyer, L. Dedet, O. Debray, *Electroencephalogr. Clin. Neurophysiol.* **46**, 310 (1979); J. J. Bouyer, M. F. Montaron, A. Rougeul, *ibid.* **51**, 244 (1981); V. N. Murthy and E. E. Fetz, *Proc. Natl. Acad. Sci. U.S.A.* **89**, 5670 (1992); J. N. Sanes and J. P. Donoghue, *ibid.* **90**, 4470 (1993).
16. For a review of spindling activity, see M. Steriade, E. G. Jones, R. R. Llinas, *Thalamic Oscillations and Signaling* (Wiley, New York, 1990).
17. M. A. L. Nicolelis, R. C. S. Lin, D. Woodward, J. K. Chapin, *Proc. Natl. Acad. Sci. U.S.A.* **90**, 2212 (1993); *Nature* **361**, 533 (1993).
18. R. P. Ericksson, *Psychol. Rev.* **75**, 447 (1968); P. S. Churchland and T. J. Sejnowski, *The Computational Brain* (MIT Press, Cambridge, MA, 1992).
19. J. K. Chapin and D. J. Woodward, *Exp. Neurol.* **78**, 654 (1982); *ibid.*, p. 670; J. D. Coulter, *J. Neurophysiol.* **37**, 831 (1973); R. J. Nelson, *Brain Res.* **304**, 143 (1984).

20. We thank L. M. O. de Oliveira, L. Andrews, H. Wiggins, G. Hetzal, and A. Kirilov for technical assistance. We thank D. Woodward for comments. This report is dedicated to Professor Cesar Timolaria. Supported by the National Institute of Dental Research (grant DE11121-01), the Whitehall Foundation, and a Whitehead Scholar Award to M.A.L.N.; NIH grant NS-26722 and Office of Naval Research grant N00014-95-1-0246 to J.K.C.; NIH grant NS-29161 to R.C.S.L.; and a doctoral fellowship from the Brazilian government (CAPES 1462-91-2) to L.A.B.

31 August 1994; accepted 6 March 1995

Stable Transfection of Malaria Parasite Blood Stages

M. R. van Dijk, A. P. Waters, C. J. Janse*

Genetic manipulation of malaria parasites would revolutionize the study of this group of pathogens and have implications for vaccine and drug development. This report describes the stable, drug-selectable genetic transformation of the clinically relevant intracellular blood stages of a malaria parasite. A plasmid transfection vector carrying the gene locus that encodes a drug-resistant form of the bifunctional enzyme dihydrofolate reductase–thymidylate synthase from the rodent malaria parasite *Plasmodium berghei* was constructed. Derivatives of this vector were introduced into merozoites of *P. berghei* by electroporation, and parasites were selected for successful transformation in the rodent host on the basis of resistance to pyrimethamine. The plasmids were present in a circular, unrearranged form that replicated episomally to an observed maximum of 15 copies per cell in drug-resistant populations.

Malaria is caused by parasitic protozoa of the genus *Plasmodium* and is annually responsible for millions of deaths, predominantly as a result of infection with *Plasmodium falciparum*. Medical research has recently concentrated on attempts to generate synthetic vaccines with the application of recombinant DNA technology or polypeptide synthesis (*1*). It is anticipated that basic research on the cellular and molecular biology of *Plasmodium* will reveal characteristics that may be exploited in disease interdiction. Recently, both transient and stable transfection protocols for genetic transformation have been described for several unicellular parasites (*2*, *3*). Although transient transfection, which has been achieved in *Plasmodium* (*4*), is useful for the investigation of the control of gene expression, it does not permit elucidation of protein function nor can it be used at present for the study of the clinically relevant blood stages.

We now describe the plasmid-mediated genetic transformation of asexual blood stages of the rodent malaria parasite *Plasmodium berghei*, based on a homologous selectable marker, the dihydrofolate reductase–thymidylate synthase (DHFR-TS) bifunctional enzyme in a drug-resistant configuration. Plasmid transfection vectors containing the gene encoding this enzyme were introduced into the parasite by electroporation. Merozoites were chosen as the initial targets because they represent the only form in the blood that exists transiently outside the erythrocyte. The use of merozoites circumvents the potential problem of electroporation-induced damage to the host erythrocyte, on which other blood stages are completely dependent for survival. Another advantage of merozoites of *P. berghei* is that they are readily collectable in large numbers and appear to be more stable than merozoites of other malaria species. Conditions of electroporation (800 V, 25 μF) similar to those used for free-living forms of unicellular parasites, including *Plasmodium* (*4*), proved effective for the introduction of DNA into *P. berghei*.

Genomic DNA (6.1 kb) from *P. berghei* containing the coding region of the DHFR-TS gene as well as 3.5 kb of upstream DNA and 1.0 kb of downstream DNA was cloned into PUC18, thereby creating the parental plasmid pMD200 (*5*). In this construct, a portion of the protein-coding region of the DHFR-TS gene was isolated from a pyrimethamine-resistant clone of *P. berghei* (*6*) that contains a point mutation that results in an amino acid replacement ($Ser^{110} \rightarrow Asn$) associated with a high level of resistance to this folic acid antagonist in both human and rodent species of malaria (*7*). A second vector, pMD204, containing only 2.5 kb of upstream DNA but identical in all other aspects of the DHFR-TS locus was also constructed in pBSKS (*5*). We assumed that the additional DNA flanking the DHFR-TS gene would provide the necessary information for the correct temporal and quantitative expression of the gene.

Two additional plasmids based on the parental plasmid pMD200 were constructed (*5*). The first, pMD221, contained a 1.8-kb fragment of the Pbs21 gene, which encodes a surface antigen of *P. berghei* ookinetes (*8*). The second plasmid, pMD223, contained 2.2 kb of the nontranscribed 2.3-kb repetitive DNA sequence specific to *P. berghei* (*9*); this repeat is present in 200 to 300 copies in the genome and is exclusively located in subtelomeric regions. These plasmids were constructed to allow for possible site-directed integration by homologous recombination into the parasite genome. The 2.3-kb repeat provides a target with a high copy number, whereas the Pbs21 gene is single copy but not transcribed as part of the asexual blood stage cycle.

In two experiments (R1 and R2), plas-

Department of Parasitology, University of Leiden, Postbus 9605, 2300RC Leiden, Netherlands.

*To whom correspondence should be addressed.